Atmos. Chem. Phys. Discuss., https://doi.org/10.5194/acp-2018-467
Manuscript under review for journal Atmos. Chem. Phys.
Discussion started: 29 May 2018

Atmospheric Chemistry and Physics Discussions

Monitoring Global Tropospheric OH Concentrations using Satellite Observations of Atmospheric Methane

Yuzhong Zhang[1,2], Daniel J. Jacob[1], Joannes D. Maasakkers[1], Melissa P. Sulprizio[1], Jian-Xiong Sheng[1], Ritesh Gautam[2], John Worden[3]

[1]School of Engineering and Applied Sciences, Harvard University, Cambridge, MA, USA
[2]Environmental Defense Fund, USA
[3]Jet Propulsion Laboratory, California Institute of Technology, Pasadena, CA, USA

Correspondence to: Yuzhong Zhang (yuzhongzhang@seas.harvard.edu)

Abstract. The hydroxyl radical (OH) is the main tropospheric oxidant and is the largest sink for atmospheric methane. The global abundance of OH has been monitored for the past decades with the methyl chloroform (CH_3CCl_3) proxy. This approach is becoming ineffective as atmospheric CH_3CCl_3 concentrations decline. Here we propose that satellite observations of atmospheric methane in the shortwave infrared (SWIR) and thermal infrared (TIR) can provide an effective replacement method. The premise is that the atmospheric signature of the methane sink from oxidation by OH is distinct from that of methane emissions. We evaluate this method in an observing system simulation experiment (OSSE) framework using synthetic SWIR and TIR satellite observations representative of the TROPOMI and CrIS instruments, respectively. The synthetic observations are interpreted with a Bayesian inverse analysis optimizing both gridded methane emissions and global OH concentrations with detailed error accounting, including errors in meteorological fields and in OH distributions. We find that the satellite observations can constrain the global tropospheric OH concentrations with a precision better than 1% and an accuracy of about 3% for SWIR and 7% for TIR. The inversion can successfully separate contributions from methane emissions and OH concentrations to the methane budget and its trend. We also show that satellite methane observations can constrain the interhemispheric difference in OH. The main limitation to the accuracy is uncertainty in the spatial and seasonal distribution of OH.

Atmos. Chem. Phys. Discuss., https://doi.org/10.5194/acp-2018-467
Manuscript under review for journal Atmos. Chem. Phys.
Discussion started: 29 May 2018

Atmospheric Chemistry and Physics Discussions

1 Introduction

The hydroxyl radical (OH) is the main oxidant in the troposphere, responsible for the oxidation of a wide range of gases including nitrogen oxides ($NO_x \equiv NO + NO_2$), sulfur dioxide (SO_2), carbon monoxide (CO), methane, and other volatile organic compounds (VOCs). Subsequent reactions can lead to the formation of tropospheric ozone, strong acids, and organic aerosol. Monitoring of global tropospheric OH concentrations and its trends is a central problem in atmospheric chemistry. Here we show that satellite observations of atmospheric methane could provide a powerful vehicle for this purpose.

The chemistry controlling tropospheric OH concentrations is complex (Levy, 1971;Logan et al., 1981). The primary source for OH is photolysis of ozone in the presence of water vapor. OH then reacts with CO and VOCs on a time scale of ~1 s to produce peroxy radicals, which can be converted back to OH by reaction with NO. This cycling of radicals is terminated by conversion to non-radical forms, principally peroxides. The dependences of OH concentrations on natural and anthropogenic emissions of NO_x, CO, and VOCs, as well as on UV radiation and humidity, are complicated and poorly established (Holmes et al., 2013;Murray et al., 2013;Monks et al., 2015).

OH concentrations are highly variable spatially and temporally, making it nearly impossible to infer global mean OH concentration from sparse direct measurements, which are difficult by themselves because of the low concentrations (~10^6 molecules cm^{-3}). Singh (1977) and Lovelock (1977) first pointed out the possibility of estimating the global mean OH concentration through atmospheric measurements of methyl chloroform (CH_3CCl_3), an industrial solvent. The industrial production of methyl chloroform is well known, and essentially all of this production is eventually released to the atmosphere, where it mixes globally in the troposphere and is removed by oxidation by OH. From measurements of atmospheric methyl chloroform and knowledge of the source, one deduces by mass balance a methyl chloroform lifetime against oxidation by tropospheric OH of 6.9 ± 0.4 years (Prather et al., 2012), providing a proxy for the global mean tropospheric OH concentration. The method became more accurate after the global ban on methyl chloroform production under the Montreal Protocol in the 1990s, as the source could then be assumed close to zero (Montzka et al., 2011). Estimates of annual and decadal OH variability can be obtained from the long-term methyl chloroform record (Prinn et al., 2001;Krol and Lelieveld, 2003;Bousquet et al., 2005;Montzka et al., 2011). Global tropospheric chemistry models tend to overestimate the OH concentrations inferred from the methyl chloroform proxy by ~ 15% (Voulgarakis et al., 2013;Naik et al., 2013) and have little success reproducing inter-annual variability and long-term trends (Holmes et al., 2013;Murray et al., 2013).

Understanding the factors controlling OH concentrations and its trends is particularly important for interpretation of methane trends. Methane is the second most important anthropogenic greenhouse gas after CO_2 and contributes to about a quarter of the climate warming experienced today (Myhre et al., 2013). About 90% of atmospheric methane is lost by reaction with OH (Kirschke et al., 2013). Atmospheric methane rose by 1-2% a^{-1} in the 1970s and 1980s, stopped growing in the late 1990s, and resumed a steady growth of 0.3-0.7% a^{-1} since 2006 (Rigby et al., 2008;Dlugokencky et al., 2009;Hartmann et al., 2013). Interpretation of these trends has generally focused on changing emissions (Rice et al., 2016;Hausmann et al., 2016;Nisbet et al., 2016;Schaefer et al., 2016), but recent studies have suggested that the growth over the past decade could be contributed by a decline in global OH concentration (Turner et al., 2017;Rigby et al., 2017). On the other hand, the trend in atmospheric CO over the past decade suggests an increase in global OH concentrations (Gaubert et al., 2017).

Inferring OH trends from methyl chloroform will become more difficult in the future as concentrations approach the detection limit (Liang et al., 2017) and evasion from the ocean complicates interpretation (Wennberg et al., 2004). Finding an alternative proxy for tropospheric OH is viewed as a pressing problem in the atmospheric chemistry community (Lelieveld et al., 2006). Huang and Prinn (2002) pointed out that the major limitation to hydrochlorofluorocarbons and hydrofluorocarbons as the alternative proxy is the lack of accurate global emission inventory. To alleviate this difficulty, Liang et al. (2017) proposed to use the hemispheric gradient of a suite of these compounds to jointly retrieve global emissions and tropospheric OH, but their approach may be limited by the sparsity of the surface observation network.

Here we propose that satellite methane observations could provide a reliable proxy for global tropospheric OH, using inverse analyses that optimize OH concentrations from the satellite data alongside with methane emission rates. Satellite measures methane in the shortwave infrared (SWIR, at 1.65 μm and 2.3 μm) by solar backscatter, and in the thermal infrared (TIR, around 7.6 μm) by terrestrial emission (Jacob et al., 2016). SWIR measurements are sensitive to the full column of methane but are mainly restricted to land, while TIR measurements are most sensitive to the middle/upper troposphere and operate over both land and ocean (Worden et al., 2015). A number of studies have used SWIR observations from the SCIAMACHY and GOSAT satellite instruments to infer methane emissions through inverse analyses. Most of these studies have assumed OH to be known (Bergamaschi et al., 2009;Spahni et al., 2011;Bergamaschi et al., 2013;Fraser et al., 2013;Monteil et al., 2013;Fraser et al., 2014;Houweling et al., 2014;Alexe et al., 2015;Pandey et al., 2015;Turner et al., 2015), while a few have optimized methane emissions together with OH concentrations using methyl chloroform measurements (Cressot et al., 2014;Cressot et al., 2016). Maasakkers et al. (2018) used six years of GOSAT data (2010-2015) to constrain methane emissions and their trends together with global OH trends.

TIR observations are of marginal value for inversion of methane emissions because they are insensitive to the boundary layer (Wecht et al., 2012) but they could provide complementary information for constraining OH. The methane sink from oxidation by OH has a distinct atmospheric signature peaking in the tropical troposphere, distributed zonally, and shifting

seasonally with the UV flux (Figure 1). The expected availability in the coming years of new high-density satellite data from TROPOMI in the SWIR (Hu et al., 2018) and CrIS in the TIR (Gambacorta et al., 2016) motivates the assessment of the potential of these data to provide a continuous means for monitoring global tropospheric OH concentrations.

2 Observing System Simulation Experiment

We conduct an observing system simulation experiment (OSSE) to examine the feasibility of inferring global tropospheric OH concentrations by inversion of satellite observations of atmospheric methane, focusing on the potential of TROPOMI (SWIR) and CrIS (TIR). The OSSE approach allows us to examine the ability of the observations to separately constrain methane emissions and OH, and to investigate the effects of errors in inversion parameters.

Figure 2 describes the structure of the OSSE. We use a chemical transport model (GEOS-Chem CTM) (Maasakkers et al., 2018) to generate a "true" global 3-D time-dependent distribution of methane concentrations, given a "true" state defined by known 2-D monthly methane emissions and 3-D monthly OH concentrations. The "true" methane concentration field is sampled following the specification of candidate satellite instruments to generate synthetic observations. We then use these synthetic observations in an inverse analysis system, with an independent CTM simulation and deliberately incorrect prior estimates of emissions and OH concentrations, to assess the capability of the observing system to retrieve the "true" state. See Brasseur and Jacob (2017) for further discussion of the OSSE approach.

The mean tropospheric OH concentration is often defined in terms of the lifetime of a long-lived gas (Prather and Spivakovsky, 1990), and in our case the natural metric is the lifetime of well-mixed methane against oxidation by tropospheric OH:

$$\tau_{\mathrm{CH_4}}^{\mathrm{OH}} = \frac{\int_{troposphere} n_a \, dv}{\int_{troposphere} k(T)[\mathrm{OH}] n_a \, dv} \quad (1)$$

where n_a is air number density, v is volume, and $k(T) = 2.45 \times 10^{-12} \mathrm{e}^{-1775/T}$ cm^3 molec^{-1} s^{-1} is the temperature-dependent oxidation rate constant (Burkholder et al., 2015). We will also examine interhemispheric differences in OH by integrating over the northern and southern hemisphere separately ($\tau_{\mathrm{CH_4}}^{\mathrm{OH,NH}}$ and $\tau_{\mathrm{CH_4}}^{\mathrm{OH,SH}}$).

2.1 Model simulation

We use the GEOS-Chem CTM to simulate atmospheric methane concentrations in the "true" atmosphere and to serve as the forward model for the inversion, with different meteorological fields and OH distributions to avoid the "fraternal twin" problem (Table 1). GEOS-Chem solves the continuity equation for atmospheric methane as

$$\frac{\partial n}{\partial \mathrm{t}} = -\nabla \cdot (n\mathbf{u}) + E - k(T) n [\mathrm{OH}] - \text{minor sinks} \quad (2)$$

where n is the methane number density, $\mathbf{u}$ is the wind vector, E is the emission field, and $k(T)$ is the rate constant for reaction with OH. Minor sinks include other tropospheric sinks (reaction with the Cl atom and soil uptake) and stratospheric sinks specified as 2-D loss rate constants. The transport term $-\nabla \cdot (n\mathbf{u})$ includes not only advection by grid-resolved winds but also parameterized subgrid convection and boundary layer mixing. The methane simulation with GEOS-Chem v11 is as described by Maasakkers et al. (2018), which builds on the previous work of Wecht et al. (2014) and Turner et al. (2015).

The GEOS-Chem simulation is conducted on a 4°×5° horizontal grid and 47 vertical layers (~ 30 layers in the troposphere). The simulation is for year 2015 with a half-year spin-up starting from June 2014 to establish methane gradients driven by synoptic-scale transport (Turner et al., 2015). We vary the state vector elements (i.e., gridded methane emission rates and global methane OH lifetime) between the "true" simulation and the inversion, to assess the ability of the inversion to improve estimations of these elements given synthetic observations. To include the effect of errors in model parameters that are not optimized in the inversion, we also vary in the inversion the model meteorological fields (for the same meteorological year) and the monthly 3-D distribution of OH.

Table 1 summarizes the OSSE conditions. The "true" emissions are taken from the GOSAT optimization of methane emissions (Maasakkers et al., 2018). The prior emissions used in the inversion are specified following Maasakkers et al. (2018), including anthropogenic (global EDGAR v4.3.2 emission inventory (European Commission, 2017) replaced with Sheng et al. (2017) in Mexico and Canada for the oil and gas sector and with Maasakkers et al. (2016) in the US), wetland (WetCHARTs v1.0 from Bloom et al. (2017)), and other sources (biomass burning, termite, and geological and geothermal seeps). The "true" global OH concentration as expressed by $\tau_{CH_4}^{OH}$ is 8.6 years with spatial/seasonal OH distribution from GEOS-Chem v5, while the prior estimate is 7.5 years with distribution from GEOS-Chem v11. The difference between the "truth" and the prior for $\tau_{CH_4}^{OH}$ is comparable to the difference between a recent observation-based analysis (Prather et al., 2012) and the mean values from current models (Naik et al., 2013;Voulgarakis et al., 2013). The OH distributions in GEOS-Chem v5 and v11 are significantly different due to many updates between these versions for lightning, isoprene chemistry, halogen chemistry, and emissions (Hu et al., 2017). In Section 4, we will consider even larger differences in OH distributions using the ACCMIP model ensemble (Naik et al., 2013).

Meteorological fields used to produce the "true" methane concentrations are the operational Goddard Earth Observing System Forward Processing (GEOS-FP) product (Lucchesi, 2017) from the NASA Global Modeling and Assimilation Office (GMAO). Meteorological fields used in the forward model for the inversion are the Modern-Era Retrospective analysis for Research and Applications, Version 2 (MERRA-2) (Gelaro et al., 2017), also produced by GMAO. GEOS-FP and MERRA-2 differ in grid resolution (cubed-sphere c720 for GEOS-FP and c360 for MERRA-2), model physics (in particular convection), and level of data assimilation and can be viewed as two independent realizations of meteorology for 2015.

Atmos. Chem. Phys. Discuss., https://doi.org/10.5194/acp-2018-467
Manuscript under review for journal Atmos. Chem. Phys.
Discussion started: 29 May 2018

2.2 Synthetic observations

Synthetic observations sample the "true" methane fields following the configurations of the satellite instrument with instrument noise added (Figure 2). Here we consider the TROPOMI instrument for SWIR and the CrIS instrument for TIR. For SWIR, the sampling is at local time 13:30 over land; and for TIR, at both 13:30 and 1:30, and over land and ocean. The retrieval success rate (ratio between the number of successful retrievals and the number of attempted retrievals) is taken to be 3% for SWIR (Hu et al., 2016) and 60% for TIR (Xiong et al., 2008) because SWIR observations require cloud-free pixels whereas TIR has tolerance for fractional cloud cover. The retrievals are for the dry air column mixing ratio X [ppb] after applying typical averaging kernels to describe vertical sensitivity (Figure 3). Gaussian random noise is added to the individual retrievals to simulate the instrument error, with a standard deviation of 0.6% for SWIR TROPOMI (Butz et al., 2012) and 2% for TIR CrIS (Gambacorta et al., 2016). To account for model biases in simulation of stratospheric methane (Patra et al., 2011) and following the recommendation of Saad et al. (2016), we replace the concentrations above 200 hPa by the 2-D seasonal climatology from ACE-FTS satellite observations (Koo et al., 2017), both in the synthetic observations and in the forward model. Our test shows that the biases in stratospheric methane concentrations resulting from different meteorological fields (MERRA-2 for the forward model and GEOS-FP for the "true" atmosphere) can lead to substantial biases in posterior estimates of $\tau_{CH_4}^{OH}$, particularly for satellite observing systems involving TIR observations. This problem is solved by imposition of the ACE-FTS stratospheric methane field.

The synthetic observations are sampled on the GEOS-Chem 4°×5° grid for the purpose of the inversion. This means that successful retrievals from individual pixels are averaged over 4°×5° grid cells and the noise is reduced by the square root of the number of successful retrievals ($N_{i,t}$) within grid cell i at time t. $N_{i,t}$ is determined as the ratio between the grid cell area (A_i) and the pixel area (a), weighted by the local cloud-free fraction ($1 - f_{i,t}$) taken from the "true" GEOS-FP meteorological fields.:

$$N_{i,t} = \left[c \times \frac{A_i \times (1 - f_{i,t})}{a} \right] \quad (3)$$

The global scaling factor c enforces the designed retrieval success rate (3% for SWIR and 60% for TIR). For a, we use the nadir resolution of SWIR TROPOMI (7×7 km^2) and TIR CrIS (14×14 km^2). The brackets [] represent the rounding function.

2.3 Inversion

We use the synthetic observations (assembled in an observation vector $\mathbf{y}$) together with the prior estimates ($\mathbf{x}_A$) and error covariance matrices for the prior ($\mathbf{S}_A$) and observations ($\mathbf{S}_O$) (Figure 2) to find the analytic solution to the inverse problem. The state vector ($\mathbf{x}$) that we seek to optimize includes annual methane emission rates on a 4°×5° grid cells for ice-free land (1009 elements) plus either 1 or 2 elements representing the global or hemispheric methane inverse lifetimes (loss

frequency). GEOS-Chem relates linearly $\mathbf{x}$ to $\mathbf{y}$ and can therefore be described for the purpose of the inversion by its Jacobian matrix $\mathbf{K} = \partial\mathbf{y}/\partial\mathbf{x}$. We compute explicitly this Jacobian matrix by perturbing the individual terms of $\mathbf{x}$ and calculating the resulting changes in $\mathbf{y}$ with GEOS-Chem.

The observation error covariance matrix $\mathbf{S_O}$ is specified as a diagonal matrix summing the instrument and forward model error variances. The instrument error is computed as described in Section 2.2. The forward model error variance is derived with the residual error method (Heald et al., 2004). Model transport error correlations (which would introduce off-diagonal terms in $\mathbf{S_O}$) can be ignored for daily or twice daily sampling on a 4°×5° grid (Heald et al., 2004). The prior error covariance matrix $\mathbf{S_A}$ is also specified as a diagonal matrix, assuming 50% error standard deviation for gridded emission rates and 10% error standard deviation for the methane inverse lifetime (Naik et al., 2013).

The Bayesian cost function for the inverse problem (Brasseur and Jacob, 2017) is

$$J(\mathbf{x}) = (\mathbf{x} - \mathbf{x_A})^{\mathrm{T}}\mathbf{S_A^{-1}}(\mathbf{x} - \mathbf{x_A}) + \gamma(\mathbf{y} - \mathbf{Kx})^{\mathrm{T}}\mathbf{S_O^{-1}}(\mathbf{y} - \mathbf{Kx}) \quad (4)$$

where γ is an adjustable regularization parameter to prevent overfitting to the observations. Analytic solution to the $J(\mathbf{x})$ minimization problem ($dJ/d\mathbf{x} = 0$) yields the posterior estimate $\hat{\mathbf{x}}$:

$$\hat{\mathbf{x}} = \mathbf{x_A} + \mathbf{G}(\mathbf{y} - \mathbf{Kx_A}) \quad (5)$$

where $\mathbf{G}$ is the gain matrix given by

$$\mathbf{G} = (\gamma\mathbf{K}^{\mathrm{T}}\mathbf{S_O^{-1}}\mathbf{K} + \mathbf{S_A^{-1}})^{-1}\gamma\mathbf{K}^{\mathrm{T}}\mathbf{S_O^{-1}} \quad (6)$$

The solution also provides a closed form of the posterior error covariance matrix ($\hat{\mathbf{S}}$):

$$\hat{\mathbf{S}} = (\gamma\mathbf{K}^{\mathrm{T}}\mathbf{S_O^{-1}}\mathbf{K} + \mathbf{S_A^{-1}})^{-1} \quad (7)$$

The diagonal elements of $\hat{\mathbf{S}}$ represents the error variances of the posterior estimates $\hat{\mathbf{x}}$.

Standard Bayesian optimization by minimizing the cost function in equation (4) with $\gamma = 1$ assumes that the observations are independent and identically distributed (IID condition) but this is generally not the case and can result in overfitting. Here we choose an optimal value for γ based on the ability of the inversion to match the "true" emissions as evaluated with the root mean square error (RMSE). Figure 4 shows that the best results (lowest RMSE) are achieved with γ in the 0.005-0.1 range and we choose here to use $\gamma = 0.0$

3 Joint Optimization of Global $\tau_{CH_4}^{OH}$ and Methane Emission Rates

Figure 5 shows the ability of the three different satellite observing systems considered (SWIR, TIR, and SWIR+TIR) to jointly constrain gridded emission rates and $\tau_{CH_4}^{OH}$. The ability to constrain emissions is measured by the RMSE on the 4o×5o

grid. The inversion with SWIR observations is able to constrain methane emissions but the one with TIR observations is not. This is consistent with the low sensitivity of TIR to the lower troposphere (Figure 3), where most of the information on spatially resolved emissions is contained. On the other hand, both SWIR and TIR are able to retrieve $\tau_{CH_4}^{OH}$ within 3% of the "true" value.

Analysis of the posterior error covariance matrix ($\hat{S}$) shows that the error standard deviations σ_p on the posterior estimate of $\tau_{CH_4}^{OH}$ are 0.75%, 0.46%, and 0.39% for SWIR, TIR, and SWIR+TIR satellite observing systems, respectively, for a one-year inversion (Table 2). $\hat{S}$ tends to be overoptimistic as a measure of posterior error because it assumes no systematic error in model parameters affecting the accuracy of the inversion (Brasseur and Jacob, 2017). Below we will explore the effect of errors in the global OH distribution as a limitation on accuracy.

A central question is the ability of the inversion to independently constrain global OH concentrations and total emissions. The error covariance between the two can be computed from $\hat{\mathbf{S}}$ (See Appendix for the method) and is visualized in Figure 6. For SWIR, the significant correlation (r = 0.78) implies some aliasing between corrections to OH concentration and emissions. Error correlation is much less (r = 0.47) with the TIR observing system. TIR observations can constrain global total emissions although they are incapable of resolving the spatial distribution of emission rates (Figure 5), and this provides a basis for successful inversion of $\tau_{CH_4}^{OH}$. The SWIR+TIR system results in smallest confidence ellipses (Figure 6) among the three satellite observing systems, suggesting that combining SWIR and TIR observations improve the ability to jointly constrain OH concentration and emissions. It should be noted that because SWIR+TIR achieves smaller errors in both $\tau_{CH_4}^{OH}$ and global total emission, the error correlation (r = 0.57) also become less consequential than the SWIR or TIR case.

To go further than the error correlation analysis, we used the OSSE environment to directly test whether perturbations to OH concentrations and global emissions can be retrieved independently. We perturbed the emission rates and/or OH concentrations in three additional simulations for the "true" atmosphere. In the first case we increased global emissions by 10%, in the second case we decreased global OH concentration by 5%, and in the third case we combined both perturbations. Figure 7 shows that the posterior estimations all correctly identify the percentage changes in global total emissions and/or OH concentration, within 2% from the "true" changes, in all three tests. This result provides evidence that our method has good ability to resolve the aliasing effect between emissions and OH on the global scale. Among all three satellite observing systems, inferred OH percentage changes with SWIR+TIR observations are closest to the "true" changes for all three cases, demonstrating that combining SWIR and TIR observations improves the ability to separate changes in OH from changes in emissions, consistent with the analysis of posterior error covariance matrices (Figure 6). The results shown in Figure 7 suggest that satellite observations of methane should be able to detect trends in OH separately from trends in methane emissions, which has important implications for attribution of trends in methane observations (Turner et al., 2017).

Atmos. Chem. Phys. Discuss., https://doi.org/10.5194/acp-2018-467
Manuscript under review for journal Atmos. Chem. Phys.
Discussion started: 29 May 2018

4 Impact of Errors in Prior OH Distributions

In our method, global OH abundance (i.e., global methane inverse lifetime) is represented by a single state vector element. The seasonal and spatial distribution of OH is a forward model parameter that the inversion does not seek to optimize. Errors in the prior OH distribution may therefore result in errors in the posterior estimate of $\tau_{CH_4}^{OH}$, which may not be fully captured by $\hat{\mathbf{S}}$. To test the impact of this uncertainty source, we use alternative "true" OH distributions from the 11 models that participated in the ACCMIP intercomparison (Naik et al., 2013), replacing GEOS-Chem v5. The ACCMIP archive includes present-day (the 2000s) 3-D monthly mean OH concentrations and was retrieved from http://badc.nerc.ac.uk/ (See Lamarque et al. (2013) for model descriptions). These models differ greatly in both global OH abundance and distribution (Figure 8). To focus on errors in OH distributions, we applied a global scaling factor to each model to impose a methane lifetime $\tau_{CH_4}^{OH}$ of 8.6 years, same as in our baseline. To avoid complicating influence from errors in the meteorological field, we do not vary the meteorological field (i.e. MERRA-2) between the "true" simulation and the inversion in this test of the sensitivity to the OH distribution.

Figure 9 shows the posterior estimation of $\tau_{CH_4}^{OH}$ resulting from the 12 different "true" OH distributions (all with the same "true" $\tau_{CH_4}^{OH}$). For all three satellite observing systems, the median posterior $\tau_{CH_4}^{OH}$ is within 2% of the "true" $\tau_{CH_4}^{OH}$. But some model OH distributions (CESM, GISS, and CICERO) result in large errors when using TIR observations. Errors are smaller for SWIR only. We determine the relative accuracy due to the uncertainty in the OH distribution (σ_a) as the ratio of the half interquartile range to the "true" $\tau_{CH_4}^{OH}$. This results in σ_a of 2.6%, 6.9%, and 6.0% for SWIR, TIR, and SWIR+TIR (Table 2). Our results suggest that satellite observing systems involving TIR measurements are likely more susceptible to errors in the OH distribution for $\tau_{CH_4}^{OH}$ estimations.

We also applied these different "true" OH distributions to the OSSE test of Figure 7 perturbing emissions and/or OH to evaluate the impact of errors in OH distribution on detecting and separating changes in global $\tau_{CH_4}^{OH}$ and emissions. The spread in inferred changes in OH is almost negligible for all the observing systems considered (Figure 7), indicating that the errors resulting from imperfect OH distribution in a single-year inversion are systematic. An important implication is that these errors from imperfect OH distribution (Figure 9) may not impair the ability to detect long-term trends in OH concentrations, as long as inter-annual variability in the OH distribution is relatively small. We therefore present them in Table 2 as a statement of accuracy.

The above results suggest that we may improve the estimation of $\tau_{CH_4}^{OH}$ if the inversion is able to retrieve information on the OH distribution from the satellite methane observations. For this purpose, we tried to optimize separately the mean OH concentrations in the northern and southern hemisphere, expressed as $\tau_{CH_4}^{OH,NH}$ and $\tau_{CH_4}^{OH,SH}$. In general, the inversion is able to

resolve the interhemispheric OH ratio ($\tau_{CH_4}^{OH,NH}/\tau_{CH_4}^{OH,SH}$) for the range of OH distributions from the different global models using both SWIR and TIR satellite observing systems (Figure 10). However, the improvement ~~in estimate of global~~ OH concentration $\tau_{CH_4}^{OH}$ (computed as harmonic mean of $\tau_{CH_4}^{OH,NH}$ and $\tau_{CH_4}^{OH,SH}$) is insignificant in most cases (not shown), indicating that errors in other factors in OH distributions (e.g., vertical and seasonal distributions) in addition to the hemispheric ratio are also important contributors to errors shown in Figure 9. A careful design of the state vector that balances the resolution of OH distribution with the aliasing of OH and emissions should further improve the accuracy of the method but is beyond the scope of the current study.

5 Conclusions

We conducted observing system simulation experiments (OSSEs) to test the feasibility of monitoring global tropospheric OH concentrations using satellite observations of methane. We considered short-wave infrared (SWIR) TROPOMI and thermal infrared (TIR) CrIS as candidate satellite instruments for this application, since methane retrievals from these instruments are expected to be available in the near future and will provide much improved coverage compared to current instruments. Through inversion of synthetic observations from these instruments sampling a "true" atmosphere, we jointly optimized gridded methane emission rates and the global tropospheric OH concentration (expressed as the methane lifetime against oxidation by tropospheric OH, $\tau_{CH_4}^{OH}$). The OSSE used different meteorological fields for the "true" atmosphere and for the inversion, and tested the effect of errors in the prior OH distributions.

Our results show that either SWIR or TIR observations can constrain $\tau_{CH_4}^{OH}$ with a precision better than 1%. Analysis of the posterior error covariance matrix shows that emissions and global OH concentrations can be separately retrieved because they have different signatures on the distribution of atmospheric methane. Simulation experiments with perturbations to either global methane emissions and/or global OH concentration demonstrate that the method can distinguish changes in OH from changes in emissions as contributors to trends in atmospheric methane. Best performance is achieved by combining the SWIR and TIR observations.

Errors in the seasonal and spatial distributions of OH assumed in the inversion of methane concentrations are the principal limitation to the accuracy in inferring the global OH concentration. Using archived OH distributions from the 12 ACCMIP models, we find that majority of the models can accurately retrieve global OH concentrations but a few are problematic when using TIR observations. Errors in the OH distribution do not degrade the ability to retrieve perturbations to OH fields and separate them from perturbations in emissions. Interhemispheric ratios of OH are also shown to be successfully constrained.

Atmos. Chem. Phys. Discuss., https://doi.org/10.5194/acp-2018-467
Manuscript under review for journal Atmos. Chem. Phys.
Discussion started: 29 May 2018

Atmospheric Chemistry and Physics Discussions

We conclude that satellite observations of methane are a promising replacement for methyl chloroform as a proxy for global tropospheric OH concentrations. Based on our OSSE ensemble results, we estimate the precision of the method to be 0.75%, 0.46%, and 0.39% and accuracy 2.6%, 6.9%, and 6.0% for SWIR, TIR, and SWIR+TIR satellite observing systems, respectively. The accuracy is limited primarily by uncertainty in the OH distribution but inference of temporal trends in OH would not be affected if any bias in the OH distribution remains constant.

Appendix

The posterior error covariance matrix ($\hat{\mathbf{S}}$) is a 1010×1010 matrix that characterizes the error covariance structure of gridded emission rates (E_i) in 1009 grid cells and global methane lifetime against oxidation by tropospheric OH ($\tau_{CH_4}^{OH}$). We condense $\hat{\mathbf{S}}$ into a 2×2 matrix $\hat{\mathbf{S}}_\mathbf{2}$, which represents the error covariance of global total emissions ($E_T = \sum_{i=1}^{n} E_i$, where n=1009) and $\tau_{CH_4}^{OH}$:

$$\hat{\mathbf{S}}_2 = \begin{bmatrix} \mathrm{Var}(E_T) & \mathrm{Cov}(E_T, \tau_{CH_4}^{OH}) \\ \mathrm{Cov}(E_T, \tau_{CH_4}^{OH}) & \mathrm{Var}(\tau_{CH_4}^{OH}) \end{bmatrix}$$

where $\mathrm{Var}(\tau_{CH_4}^{OH})$ can be directly obtained from $\hat{\mathbf{S}}$, and $\mathrm{Var}(E_T)$ and $\mathrm{Cov}(E_T, \tau_{CH_4}^{OH})$ can be computed from $\hat{\mathbf{S}}$ with the following formulae:

$$\mathrm{Var}(E_T) = \sum_{i=1}^{n} \mathrm{Var}(E_i) + 2 \sum_{1 \le i < j \le n} \mathrm{Cov}(E_i, E_j)$$

$$\mathrm{Cov}(E_T, \tau_{CH_4}^{OH}) = \sum_{i=1}^{n} \mathrm{Cov}(E_i, \tau_{CH_4}^{OH})$$

$\hat{\mathbf{S}}_2$ can then be visualized as a bi-variate Gaussian distribution.

Acknowledgments. This work was funded by the Interdisciplinary Science (IDS) program of the NASA Earth Science Division. Y. Zhang was partially funded by the Kravis Scientific Research Fund at Environmental Defense Fund.

References

Alexe, M., Bergamaschi, P., Segers, A., Detmers, R., Butz, A., Hasekamp, O., Guerlet, S., Parker, R., Boesch, H., Frankenberg, C., Scheepmaker, R. A., Dlugokencky, E., Sweeney, C., Wofsy, S. C., and Kort, E. A.: Inverse modelling of CH_4 emissions for 2010–2011 using different satellite retrieval products from GOSAT and SCIAMACHY, Atmos. Chem. Phys., 15, 113-133, 10.5194/acp-15-113-2015, 2015.

Bergamaschi, P., Frankenberg, C., Meirink, J. F., Krol, M., Villani, M. G., Houweling, S., Dentener, F., Dlugokencky, E. J., Miller, J. B., Gatti, L. V., Engel, A., and Levin, I.: Inverse modeling of global and regional CH_4 emissions using SCIAMACHY satellite retrievals, Journal of Geophysical Research: Atmospheres, 114, D22301, 10.1029/2009JD012287, 2009.

Bergamaschi, P., Houweling, S., Segers, A., Krol, M., Frankenberg, C., Scheepmaker, R. A., Dlugokencky, E., Wofsy, S. C., Kort, E. A., Sweeney, C., Schuck, T., Brenninkmeijer, C., Chen, H., Beck, V., and Gerbig, C.: Atmospheric CH_4 in the first decade of the 21st century: Inverse modeling analysis using SCIAMACHY satellite retrievals and NOAA surface measurements, Journal of Geophysical Research: Atmospheres, 118, 7350-7369, 10.1002/jgrd.50480, 2013.

Bloom, A. A., Bowman, K. W., Lee, M., Turner, A. J., Schroeder, R., Worden, J. R., Weidner, R., McDonald, K. C., and Jacob, D. J.: A global wetland methane emissions and uncertainty dataset for atmospheric chemical transport models (WetCHARTs version 1.0), Geosci. Model Dev., 10, 2141-2156, 10.5194/gmd-10-2141-2017, 2017.

Bousquet, P., Hauglustaine, D. A., Peylin, P., Carouge, C., and Ciais, P.: Two decades of OH variability as inferred by an inversion of atmospheric transport and chemistry of methyl chloroform, Atmos. Chem. Phys., 5, 2635-2656, 10.5194/acp-5-2635-2005, 2005.

Brasseur, G. P., and Jacob, D. J.: Modeling of Atmospheric Chemistry, Cambridge University Press, Cambridge, 2017.

Burkholder, J. B., Sander, S. P., Abbatt, J., Barker, J. R., Huie, R. E., Kolb, C. E., Kurylo, M. J., Orkin, V. L., Wilmouth, D. M., and Wine, P. H.: Chemical Kinetics and Photochemical Data for Use in Atmospheric Studies, Evaluation No. 18, Jet Propulsion Laboratory, Pasadena, 2015.

Butz, A., Galli, A., Hasekamp, O., Landgraf, J., Tol, P., and Aben, I.: TROPOMI aboard Sentinel-5 Precursor: Prospective performance of CH_4 retrievals for aerosol and cirrus loaded atmospheres, Remote Sensing of Environment, 120, 267-276, https://doi.org/10.1016/j.rse.2011.05.030, 2012.

European Commission, Joint Research Centre (JRC)/Netherlands Environmental Assessment Agency (PBL): Emission Database for Global Atmospheric Research (EDGAR), release version 4.3.2, http://edgar.jrc.ec.europa.eu/overview.php?v=432, 2017.

Cressot, C., Chevallier, F., Bousquet, P., Crevoisier, C., Dlugokencky, E. J., Fortems-Cheiney, A., Frankenberg, C., Parker, R., Pison, I., Scheepmaker, R. A., Montzka, S. A., Krummel, P. B., Steele, L. P., and Langenfelds, R. L.: On the consistency between global and regional methane emissions inferred from SCIAMACHY, TANSO-FTS, IASI and surface measurements, Atmos. Chem. Phys., 14, 577-592, 10.5194/acp-14-577-2014, 2014.

Cressot, C., Pison, I., Rayner, P. J., Bousquet, P., Fortems-Cheiney, A., and Chevallier, F.: Can we detect regional methane anomalies? A comparison between three observing systems, Atmos. Chem. Phys., 16, 9089-9108, 10.5194/acp-16-9089-2016, 2016.

Dlugokencky, E. J., Bruhwiler, L., White, J. W. C., Emmons, L. K., Novelli, P. C., Montzka, S. A., Masarie, K. A., Lang, P. M., Crotwell, A. M., Miller, J. B., and Gatti, L. V.: Observational constraints on recent increases in the atmospheric CH_4 burden, Geophysical Research Letters, 36, L18803, 10.1029/2009GL039780, 2009.

Fraser, A., Palmer, P. I., Feng, L., Boesch, H., Cogan, A., Parker, R., Dlugokencky, E. J., Fraser, P. J., Krummel, P. B., Langenfelds, R. L., O'Doherty, S., Prinn, R. G., Steele, L. P., van der Schoot, M., and Weiss, R. F.: Estimating regional methane surface fluxes: the relative importance of surface and GOSAT mole fraction measurements, Atmos. Chem. Phys., 13, 5697-5713, 10.5194/acp-13-5697-2013, 2013.

Fraser, A., Palmer, P. I., Feng, L., Bösch, H., Parker, R., Dlugokencky, E. J., Krummel, P. B., and Langenfelds, R. L.: Estimating regional fluxes of CO_2 and CH_4 using space-borne observations of XCH_4: XCO_2, Atmos. Chem. Phys., 14, 12883-12895, 10.5194/acp-14-12883-2014, 2014.

Gambacorta, A., Barnet, C., Smith, N., Pierce, B., Smith, J., Spackman, R., and Goldberg, M.: The NPP and J1 NOAA Unique Combined Atmospheric Processing System (NUCAPS) for atmospheric thermal sounding: recent algorithm enhancements tailored to near real time users applications, the American Geophysical Union Fall 2016 meeting, San Francisco, California, 2016.

Gaubert, B., Worden, H. M., Arellano, A. F. J., Emmons, L. K., Tilmes, S., Barré, J., Martinez Alonso, S., Vitt, F., Anderson, J. L., Alkemade, F., Houweling, S., and Edwards, D. P.: Chemical Feedback From Decreasing Carbon Monoxide Emissions, Geophysical Research Letters, 44, 9985-9995, 10.1002/2017GL074987, 2017.

Gelaro, R., McCarty, W., Suárez, M. J., Todling, R., Molod, A., Takacs, L., Randles, C. A., Darmenov, A., Bosilovich, M. G., Reichle, R., Wargan, K., Coy, L., Cullather, R., Draper, C., Akella, S., Buchard, V., Conaty, A., Silva, A. M. d., Gu, W., Kim, G.-K., Koster, R., Lucchesi, R., Merkova, D., Nielsen, J. E., Partyka, G., Pawson, S., Putman, W., Rienecker, M., Schubert, S. D., Sienkiewicz, M., and Zhao, B.: The Modern-Era Retrospective Analysis for Research and Applications, Version 2 (MERRA-2), Journal of Climate, 30, 5419-5454, 10.1175/jcli-d-16-0758.1, 2017.

Hartmann, D. L., Klein Tank, A. M. G., Rusticucci, M., Alexander, L. V., Brönnimann, S., Charabi, Y., Dentener, F. J., Dlugokencky, E. J., Easterling, D. R., Kaplan, A., Soden, B. J., Thorne, P. W., Wild, M., and Zhai, P. M.: Observations: Atmosphere and Surface, in: Climate Change 2013: The Physical Science Basis. Contribution of Working Group I to the Fifth Assessment Report of the Intergovernmental Panel on Climate Change, edited by: Stocker, T. F., Qin, D., Plattner, G.-K., Tignor, M., Allen, S. K., Boschung, J., Nauels, A., Xia, Y., Bex, V., and Midgley, P. M., Cambridge University Press, Cambridge, United Kingdom and New York, NY, USA, 159-254, 2013.

Hausmann, P., Sussmann, R., and Smale, D.: Contribution of oil and natural gas production to renewed increase in atmospheric methane (2007–2014): top–down estimate from ethane and methane column observations, Atmos. Chem. Phys., 16, 3227-3244, 10.5194/acp-16-3227-2016, 2016.

Heald, C. L., Jacob, D. J., Jones, D. B. A., Palmer, P. I., Logan, J. A., Streets, D. G., Sachse, G. W., Gille, J. C., Hoffman, R. N., and Nehrkorn, T.: Comparative inverse analysis of satellite (MOPITT) and aircraft (TRACE-P) observations to estimate Asian sources of carbon monoxide, Journal of Geophysical Research: Atmospheres, 109, D23306, 10.1029/2004JD005185, 2004.

Holmes, C. D., Prather, M. J., Søvde, O. A., and Myhre, G.: Future methane, hydroxyl, and their uncertainties: key climate and emission parameters for future predictions, Atmos. Chem. Phys., 13, 285-302, 10.5194/acp-13-285-2013, 2013.

Houweling, S., Krol, M., Bergamaschi, P., Frankenberg, C., Dlugokencky, E. J., Morino, I., Notholt, J., Sherlock, V., Wunch, D., Beck, V., Gerbig, C., Chen, H., Kort, E. A., Röckmann, T., and Aben, I.: A multi-year methane inversion using SCIAMACHY, accounting for systematic errors using TCCON measurements, Atmos. Chem. Phys., 14, 3991-4012, 10.5194/acp-14-3991-2014, 2014.

Hu, H., Hasekamp, O., Butz, A., Galli, A., Landgraf, J., Aan de Brugh, J., Borsdorff, T., Scheepmaker, R., and Aben, I.: The operational methane retrieval algorithm for TROPOMI, Atmos. Meas. Tech., 9, 5423-5440, 10.5194/amt-9-5423-2016, 2016.

Hu, H., Landgraf, J., Detmers, R., Borsdorff, T., AandeBrugh, J., Aben, I., Butz, A., and Hasekamp, O. P.: Toward global mapping of methane with TROPOMI: first results and intersatellite comparison to GOSAT, Geophys. Res. Lett., 45, 10.1002/2018GL077259, 2018.

Hu, L., Jacob, D. J., Liu, X., Zhang, Y., Zhang, L., Kim, P. S., Sulprizio, M. P., and Yantosca, R. M.: Global budget of tropospheric ozone: Evaluating recent model advances with satellite (OMI), aircraft (IAGOS), and ozonesonde observations, Atmospheric Environment, 167, 323-334, https://doi.org/10.1016/j.atmosenv.2017.08.036, 2017.

Huang, J., and Prinn, R. G.: Critical evaluation of emissions of potential new gases for OH estimation, Journal of Geophysical Research: Atmospheres, 107, ACH 18-11-ACH 18-12, doi:10.1029/2002JD002394, 2002.

Jacob, D. J., Turner, A. J., Maasakkers, J. D., Sheng, J., Sun, K., Liu, X., Chance, K., Aben, I., McKeever, J., and Frankenberg, C.: Satellite observations of atmospheric methane and their value for quantifying methane emissions, Atmos. Chem. Phys., 16, 14371-14396, 10.5194/acp-16-14371-2016, 2016.

Kirschke, S., Bousquet, P., Ciais, P., Saunois, M., Canadell, J. G., Dlugokencky, E. J., Bergamaschi, P., Bergmann, D., Blake, D. R., Bruhwiler, L., Cameron-Smith, P., Castaldi, S., Chevallier, F., Feng, L., Fraser, A., Heimann, M., Hodson, E. L., Houweling, S., Josse, B., Fraser, P. J., Krummel, P. B., Lamarque, J.-F., Langenfelds, R. L., Le Quéré, C., Naik, V., O'Doherty, S., Palmer, P. I., Pison, I., Plummer, D., Poulter, B., Prinn, R. G., Rigby, M., Ringeval, B., Santini, M., Schmidt, M., Shindell, D. T., Simpson, I. J., Spahni, R., Steele, L. P., Strode, S. A., Sudo, K., Szopa, S., van der Werf, G. R., Voulgarakis, A., van Weele, M., Weiss, R. F., Williams, J. E., and Zeng, G.: Three decades of global methane sources and sinks, Nature Geoscience, 6, 813, 10.1038/ngeo1955
https://www.nature.com/articles/ngeo1955 - supplementary-information, 2013.

Koo, J.-H., Walker, K. A., Jones, A., Sheese, P. E., Boone, C. D., Bernath, P. F., and Manney, G. L.: Global climatology based on the ACE-FTS version 3.5 dataset: Addition of mesospheric levels and carbon-containing species in the UTLS, Journal of Quantitative Spectroscopy and Radiative Transfer, 186, 52-62, 10.1016/j.jqsrt.2016.07.003, 2017.

Krol, M., and Lelieveld, J.: Can the variability in tropospheric OH be deduced from measurements of 1,1,1-trichloroethane (methyl chloroform)?, Journal of Geophysical Research: Atmospheres, 108, n/a-n/a, 10.1029/2002JD002423, 2003.

Lamarque, J. F., Shindell, D. T., Josse, B., Young, P. J., Cionni, I., Eyring, V., Bergmann, D., Cameron-Smith, P., Collins, W. J., Doherty, R., Dalsoren, S., Faluvegi, G., Folberth, G., Ghan, S. J., Horowitz, L. W., Lee, Y. H., MacKenzie, I. A., Nagashima, T., Naik, V., Plummer, D., Righi, M., Rumbold, S. T., Schulz, M., Skeie, R. B., Stevenson, D. S., Strode, S., Sudo, K., Szopa, S., Voulgarakis, A., and Zeng, G.: The Atmospheric Chemistry and Climate Model Intercomparison Project (ACCMIP): overview and description of models, simulations and climate diagnostics, Geosci. Model Dev., 6, 179-206, 10.5194/gmd-6-179-2013, 2013.

Lelieveld, J., Brenninkmeijer, C. A. M., Joeckel, P., Isaksen, I. S. A., Krol, M. C., Mak, J. E., Dlugokencky, E., Montzka, S. A., Novelli, P. C., Peters, W., and Tans, P. P.: New Directions: Watching over tropospheric hydroxyl (OH), Atmospheric Environment, 40, 5741-5743, https://doi.org/10.1016/j.atmosenv.2006.04.008, 2006.

Levy, H.: Normal Atmosphere: Large Radical and Formaldehyde Concentrations Predicted, Science, 173, 141-143, 10.1126/science.173.3992.141, 1971.

Liang, Q., Chipperfield, M. P., Fleming, E. L., Luke Abraham, N., Braesicke, P., Burkholder, J. B., Daniel, J. S., Dhomse, S., Fraser, P. J., Hardiman, S. C., Jackman, C. H., Kinnison, D. E., Krummel, P. B., Montzka, S. A., Morgenstern, O., McCulloch, A., Mühle, J., Newman, P. A., Orkin, V. L., Pitari, G., Prinn, R. G., Rigby, M., Rozanov, E., Stenke, A., Tummon, F., Velders, G. J. M., Visioni, D., and Weiss, R. F.: Deriving global OH abundance and atmospheric lifetimes for long-lived gases: A search for CH_3CCl_3 alternatives, Journal of Geophysical Research: Atmospheres, n/a-n/a, 10.1002/2017JD026926, 2017.

Logan, J. A., Prather, M. J., Wofsy, S. C., and McElroy, M. B.: Tropospheric chemistry: A global perspective, Journal of Geophysical Research: Oceans, 86, 7210-7254, 10.1029/JC086iC08p07210, 1981.

Lovelock, J. E.: Methyl chloroform in the troposphere as an indicator of OH radical abundance, Nature, 267, 32-32, 1977.

Lucchesi, R.: File Specification for GEOS-5 FP. GMAO Office Note NO. 4 (Version 1.1), 61, 2017.

Maasakkers, J. D., Jacob, D. J., Sulprizio, M. P., Turner, A. J., Weitz, M., Wirth, T., Hight, C., DeFigueiredo, M., Desai, M., Schmeltz, R., Hockstad, L., Bloom, A. A., Bowman, K. W., Jeong, S., and Fischer, M. L.: Gridded National Inventory of U.S. Methane Emissions, Environmental Science & Technology, 50, 13123-13133, 10.1021/acs.est.6b02878, 2016.

Maasakkers, J. D., Jacob, D. J., Sulprizio, M. P., Hersher, M., Scarpelli, T., Turner, A. J., Sheng, J., Bloom, A., Bowman, K., and Parker, R.: Global distribution of methane emissions, emission trends, and OH trends inferred from an inversion of GOSAT data for 2010-2015, in preparation, 2018.

Monks, S. A., Arnold, S. R., Emmons, L. K., Law, K. S., Turquety, S., Duncan, B. N., Flemming, J., Huijnen, V., Tilmes, S., Langner, J., Mao, J., Long, Y., Thomas, J. L., Steenrod, S. D., Raut, J. C., Wilson, C., Chipperfield, M. P., Diskin, G. S.,

Weinheimer, A., Schlager, H., and Ancellet, G.: Multi-model study of chemical and physical controls on transport of anthropogenic and biomass burning pollution to the Arctic, Atmos. Chem. Phys., 15, 3575-3603, 10.5194/acp-15-3575-2015, 2015.

Monteil, G., Houweling, S., Butz, A., Guerlet, S., Schepers, D., Hasekamp, O., Frankenberg, C., Scheepmaker, R., Aben, I., and Röckmann, T.: Comparison of CH4 inversions based on 15 months of GOSAT and SCIAMACHY observations, Journal of Geophysical Research: Atmospheres, 118, 11,807-811,823, 10.1002/2013JD019760, 2013.

Montzka, S. A., Krol, M., Dlugokencky, E., Hall, B., Jöckel, P., and Lelieveld, J.: Small Interannual Variability of Global Atmospheric Hydroxyl, Science, 331, 67, 2011.

Murray, L. T., Logan, J. A., and Jacob, D. J.: Interannual variability in tropical tropospheric ozone and OH: The role of lightning, Journal of Geophysical Research: Atmospheres, 118, 11,468-411,480, 10.1002/jgrd.50857, 2013.

Myhre, G., Shindell, D., Bréon, F.-M., Collins, W., Fuglestvedt, J., Huang, J., Koch, D., Lamarque, J.-F., Lee, D., and Mendoza, B.: Anthropogenic and natural radiative forcing, Climate change, 423, 658-740, 2013.

Naik, V., Voulgarakis, A., Fiore, A. M., Horowitz, L. W., Lamarque, J. F., Lin, M., Prather, M. J., Young, P. J., Bergmann, D., Cameron-Smith, P. J., Cionni, I., Collins, W. J., Dalsøren, S. B., Doherty, R., Eyring, V., Faluvegi, G., Folberth, G. A., Josse, B., Lee, Y. H., MacKenzie, I. A., Nagashima, T., van Noije, T. P. C., Plummer, D. A., Righi, M., Rumbold, S. T., Skeie, R., Shindell, D. T., Stevenson, D. S., Strode, S., Sudo, K., Szopa, S., and Zeng, G.: Preindustrial to present-day changes in tropospheric hydroxyl radical and methane lifetime from the Atmospheric Chemistry and Climate Model Intercomparison Project (ACCMIP), Atmos. Chem. Phys., 13, 5277-5298, 10.5194/acp-13-5277-2013, 2013.

Nisbet, E. G., Dlugokencky, E. J., Manning, M. R., Lowry, D., Fisher, R. E., France, J. L., Michel, S. E., Miller, J. B., White, J. W. C., Vaughn, B., Bousquet, P., Pyle, J. A., Warwick, N. J., Cain, M., Brownlow, R., Zazzeri, G., Lanoisellé, M., Manning, A. C., Gloor, E., Worthy, D. E. J., Brunke, E. G., Labuschagne, C., Wolff, E. W., and Ganesan, A. L.: Rising atmospheric methane: 2007–2014 growth and isotopic shift, Global Biogeochemical Cycles, 30, 1356-1370, 10.1002/2016GB005406, 2016.

Pandey, S., Houweling, S., Krol, M., Aben, I., and Röckmann, T.: On the use of satellite-derived CH_4: CO_2 columns in a joint inversion of CH_4 and CO_2 fluxes, Atmos. Chem. Phys., 15, 8615-8629, 10.5194/acp-15-8615-2015, 2015.

Patra, P. K., Houweling, S., Krol, M., Bousquet, P., Belikov, D., Bergmann, D., Bian, H., Cameron-Smith, P., Chipperfield, M. P., Corbin, K., Fortems-Cheiney, A., Fraser, A., Gloor, E., Hess, P., Ito, A., Kawa, S. R., Law, R. M., Loh, Z., Maksyutov, S., Meng, L., Palmer, P. I., Prinn, R. G., Rigby, M., Saito, R., and Wilson, C.: TransCom model simulations of CH_4 and related species: linking transport, surface flux and chemical loss with CH_4 variability in the troposphere and lower stratosphere, Atmos. Chem. Phys., 11, 12813-12837, 10.5194/acp-11-12813-2011, 2011.

Prather, M., and Spivakovsky, C. M.: Tropospheric OH and the lifetimes of hydrochlorofluorocarbons, Journal of Geophysical Research: Atmospheres, 95, 18723-18729, doi:10.1029/JD095iD11p18723, 1990.

Prather, M. J., Holmes, C. D., and Hsu, J.: Reactive greenhouse gas scenarios: Systematic exploration of uncertainties and the role of atmospheric chemistry, Geophysical Research Letters, 39, L09803, 10.1029/2012GL051440, 2012.

Prinn, R. G., Huang, J., Weiss, R. F., Cunnold, D. M., Fraser, P. J., Simmonds, P. G., McCulloch, A., Harth, C., Salameh, P., Doherty, S., Wang, R. H. J., Porter, L., and Miller, B. R.: Evidence for Substantial Variations of Atmospheric Hydroxyl Radicals in the Past Two Decades, Science, 292, 1882, 2001.

Rice, A. L., Butenhoff, C. L., Teama, D. G., Röger, F. H., Khalil, M. A. K., and Rasmussen, R. A.: Atmospheric methane isotopic record favors fossil sources flat in 1980s and 1990s with recent increase, Proceedings of the National Academy of Sciences, 113, 10791-10796, 10.1073/pnas.1522923113, 2016.

Rigby, M., Prinn, R. G., Fraser, P. J., Simmonds, P. G., Langenfelds, R. L., Huang, J., Cunnold, D. M., Steele, L. P., Krummel, P. B., Weiss, R. F., O'Doherty, S., Salameh, P. K., Wang, H. J., Harth, C. M., Mühle, J., and Porter, L. W.: Renewed growth of atmospheric methane, Geophysical Research Letters, 35, L22805, 10.1029/2008GL036037, 2008.

Rigby, M., Montzka, S. A., Prinn, R. G., White, J. W. C., Young, D., O'Doherty, S., Lunt, M. F., Ganesan, A. L., Manning, A. J., Simmonds, P. G., Salameh, P. K., Harth, C. M., Mühle, J., Weiss, R. F., Fraser, P. J., Steele, L. P., Krummel, P. B., McCulloch, A., and Park, S.: Role of atmospheric oxidation in recent methane growth, Proceedings of the National Academy of Sciences, 114, 5373-5377, 10.1073/pnas.1616426114, 2017.

Saad, K. M., Wunch, D., Deutscher, N. M., Griffith, D. W. T., Hase, F., De Mazière, M., Notholt, J., Pollard, D. F., Roehl, C. M., Schneider, M., Sussmann, R., Warneke, T., and Wennberg, P. O.: Seasonal variability of stratospheric methane: implications for constraining tropospheric methane budgets using total column observations, Atmos. Chem. Phys., 16, 14003-14024, 10.5194/acp-16-14003-2016, 2016.

Schaefer, H., Fletcher, S. E. M., Veidt, C., Lassey, K. R., Brailsford, G. W., Bromley, T. M., Dlugokencky, E. J., Michel, S. E., Miller, J. B., Levin, I., Lowe, D. C., Martin, R. J., Vaughn, B. H., and White, J. W. C.: A 21st century shift from fossil-fuel to biogenic methane emissions indicated by $^{13}CH_4$, Science, 10.1126/science.aad2705, 2016.

Sheng, J.-X., Jacob, D. J., Maasakkers, J. D., Sulprizio, M. P., Zavala-Araiza, D., and Hamburg, S. P.: A high-resolution ($0.1^o \times 0.1^o$) inventory of methane emissions from Canadian and Mexican oil and gas systems, Atmospheric Environment, 158, 211-215, https://doi.org/10.1016/j.atmosenv.2017.02.036, 2017.

Singh, H. B.: Preliminary estimation of average tropospheric HO concentrations in the northern and southern hemispheres, Geophysical Research Letters, 4, 453-456, 10.1029/GL004i010p00453, 1977.

Spahni, R., Wania, R., Neef, L., van Weele, M., Pison, I., Bousquet, P., Frankenberg, C., Foster, P. N., Joos, F., Prentice, I. C., and van Velthoven, P.: Constraining global methane emissions and uptake by ecosystems, Biogeosciences, 8, 1643-1665, 10.5194/bg-8-1643-2011, 2011.

Turner, A. J., Jacob, D. J., Wecht, K. J., Maasakkers, J. D., Lundgren, E., Andrews, A. E., Biraud, S. C., Boesch, H., Bowman, K. W., Deutscher, N. M., Dubey, M. K., Griffith, D. W. T., Hase, F., Kuze, A., Notholt, J., Ohyama, H., Parker, R., Payne, V. H., Sussmann, R., Sweeney, C., Velazco, V. A., Warneke, T., Wennberg, P. O., and Wunch, D.: Estimating global and North American methane emissions with high spatial resolution using GOSAT satellite data, Atmos. Chem. Phys., 15, 7049-7069, 10.5194/acp-15-7049-2015, 2015.

Turner, A. J., Frankenberg, C., Wennberg, P. O., and Jacob, D. J.: Ambiguity in the causes for decadal trends in atmospheric methane and hydroxyl, Proceedings of the National Academy of Sciences, 114, 5367-5372, 10.1073/pnas.1616020114, 2017.

Voulgarakis, A., Naik, V., Lamarque, J. F., Shindell, D. T., Young, P. J., Prather, M. J., Wild, O., Field, R. D., Bergmann, D., Cameron-Smith, P., Cionni, I., Collins, W. J., Dalsøren, S. B., Doherty, R. M., Eyring, V., Faluvegi, G., Folberth, G. A., Horowitz, L. W., Josse, B., MacKenzie, I. A., Nagashima, T., Plummer, D. A., Righi, M., Rumbold, S. T., Stevenson, D. S., Strode, S. A., Sudo, K., Szopa, S., and Zeng, G.: Analysis of present day and future OH and methane lifetime in the ACCMIP simulations, Atmos. Chem. Phys., 13, 2563-2587, 10.5194/acp-13-2563-2013, 2013.

Wecht, K. J., Jacob, D. J., Wofsy, S. C., Kort, E. A., Worden, J. R., Kulawik, S. S., Henze, D. K., Kopacz, M., and Payne, V. H.: Validation of TES methane with HIPPO aircraft observations: implications for inverse modeling of methane sources, Atmos. Chem. Phys., 12, 1823-1832, 10.5194/acp-12-1823-2012, 2012.

Wecht, K. J., Jacob, D. J., Frankenberg, C., Jiang, Z., and Blake, D. R.: Mapping of North American methane emissions with high spatial resolution by inversion of SCIAMACHY satellite data, Journal of Geophysical Research: Atmospheres, 119, 7741-7756, 10.1002/2014JD021551, 2014.

Wennberg, P. O., Peacock, S., Randerson, J. T., and Bleck, R.: Recent changes in the air-sea gas exchange of methyl chloroform, Geophysical Research Letters, 31, n/a-n/a, 10.1029/2004GL020476, 2004.

Worden, J. R., Turner, A. J., Bloom, A., Kulawik, S. S., Liu, J., Lee, M., Weidner, R., Bowman, K., Frankenberg, C., Parker, R., and Payne, V. H.: Quantifying lower tropospheric methane concentrations using GOSAT near-IR and TES thermal IR measurements, Atmos. Meas. Tech., 8, 3433-3445, 10.5194/amt-8-3433-2015, 2015.

Xiong, X., Barnet, C., Maddy, E., Sweeney, C., Liu, X., Zhou, L., and Goldberg, M.: Characterization and validation of methane products from the Atmospheric Infrared Sounder (AIRS), Journal of Geophysical Research: Biogeosciences, 113, G00A01, 10.1029/2007JG000500, 2008.

Atmos. Chem. Phys. Discuss., https://doi.org/10.5194/acp-2018-467
Manuscript under review for journal Atmos. Chem. Phys.
Discussion started: 29 May 2018

Table 1 OSSE conditions.

	"True" Atmosphere	Inversion Prior and Parameters
State Vector (**x**)		
Gridded Emission Rates [a]	Posterior from GOSAT analysis[b]	EDGAR v4.3.2+ WetCHARTs[c]
Global OH concentration ($\tau_{CH_4}^{OH}$) [d]	8.6 years	7.5 years
Parameters		
OH Distribution	GEOS-Chem v5 [e]	GEOS-Chem v11
Meteorological Field [f]	GEOS-FP	MERRA-2

[a] Methane emission rates on a 4°×5° grid over ice-free land (1009 elements).

[b] From Maasakkers et al. (2018).

[c] Prior emissions are specified following Maasakkers et al. (2018). EDGAR v4.3.2 (European Commission, 2017) is used as the global default for anthropogenic emissions, but is replaced with Sheng et al. (2017) in Mexico and Canada for the oil and gas sector and Maasakkers et al. (2016) in the US. WetCHARTs is from Bloom et al. (2017). Sources from biomass burning, termite, and geological seeps are also specified with available emission inventories.

[d] Expressed as methane lifetime against oxidation by tropospheric OH (equation (1)).

[e] Sensitivity simulations in Section 4 use 11 global OH distributions from the ACCMIP ensemble (Naik et al., 2013).

[f] Meteorological fields are for 2015.

Atmos. Chem. Phys. Discuss., https://doi.org/10.5194/acp-2018-467
Manuscript under review for journal Atmos. Chem. Phys.
Discussion started: 29 May 2018

Atmospheric Chemistry and Physics Discussions

Table 2 Uncertainty in $\tau_{CH_4}^{OH}$ estimations with different satellite observing systems.

Observing System	SWIR	TIR	SWIR+TIR
Precision (σ_p)	0.75%	0.46%	0.39%
Accuracy (σ_a) [a]	2.6%	6.9%	6.0%

[a] Accuracy is derived from inversions using different OH distributions from 12 global models for the "true" atmosphere (Section 4).

5

Atmos. Chem. Phys. Discuss., https://doi.org/10.5194/acp-2018-467
Manuscript under review for journal Atmos. Chem. Phys.
Discussion started: 29 May 2018

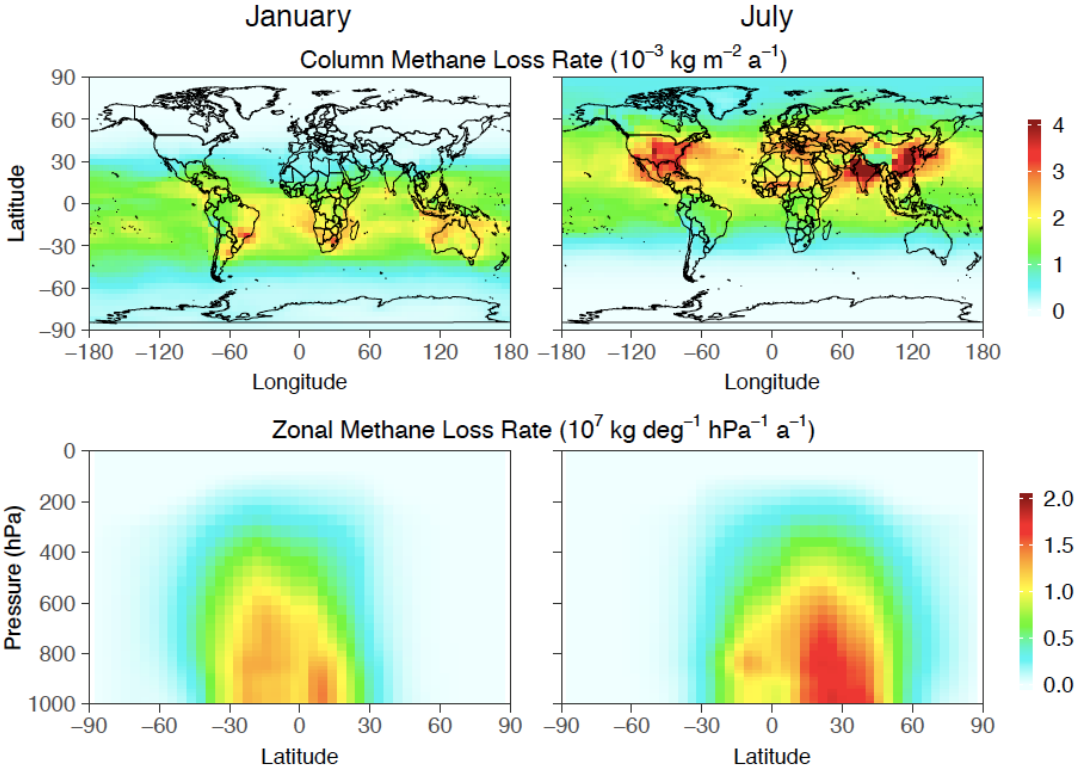

Figure 1 Monthly methane loss rate from oxidation by OH in January and July 2015 computed with the GEOS-Chem model (Maasakkers et al., 2018). The top panels show the column loss rates and the bottom panels show the zonal loss rates.

Atmos. Chem. Phys. Discuss., https://doi.org/10.5194/acp-2018-467
Manuscript under review for journal Atmos. Chem. Phys.
Discussion started: 29 May 2018

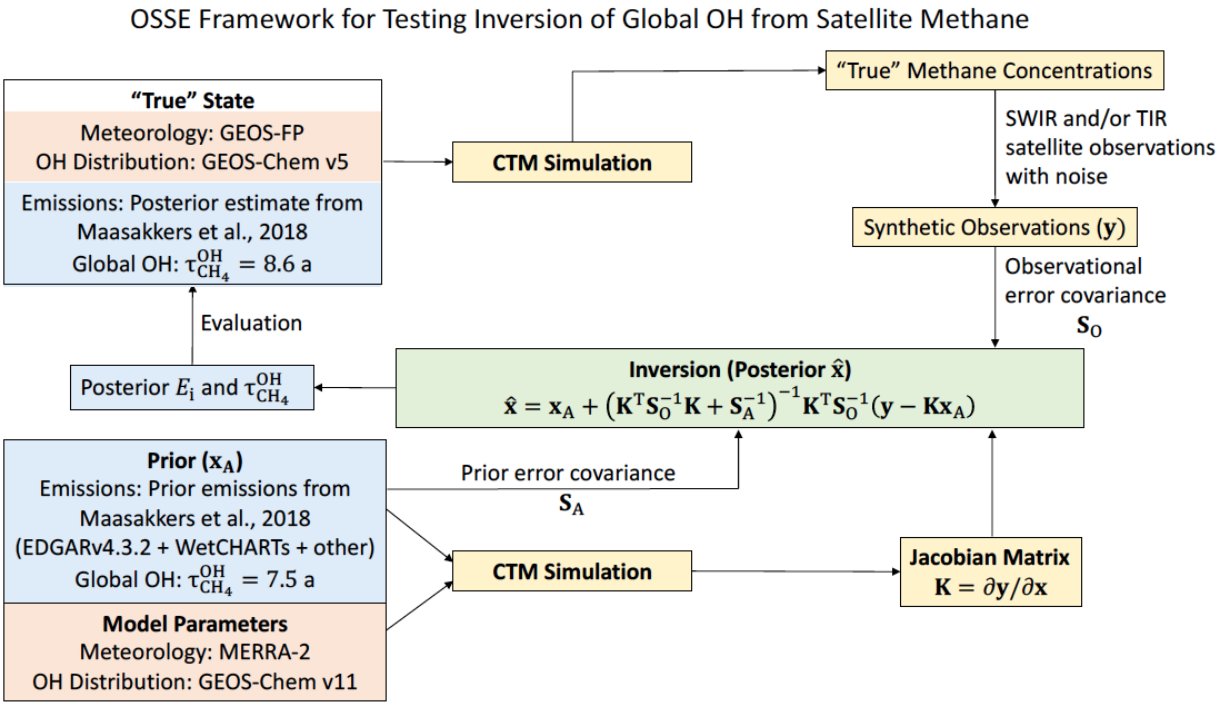

Figure 2 Observing System Simulation Experiment (OSSE) framework to test the ability of SWIR and TIR satellite observations of atmospheric methane to simultaneously constrain methane emission rates (E_i) and the global mean tropospheric OH concentration expressed as methane lifetime against oxidation by tropospheric OH ($\tau_{CH_4}^{OH}$).

Atmos. Chem. Phys. Discuss., https://doi.org/10.5194/acp-2018-467
Manuscript under review for journal Atmos. Chem. Phys.
Discussion started: 29 May 2018

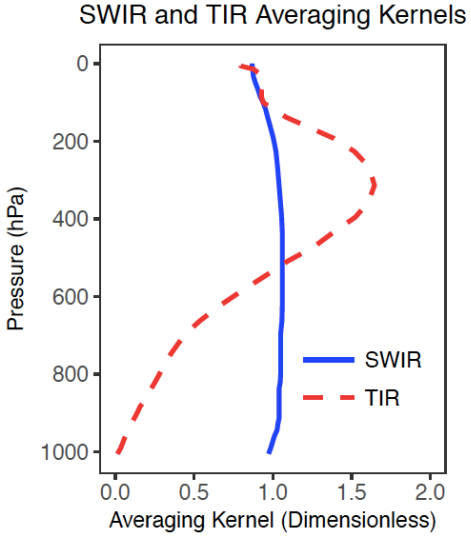

Figure 3 Typical vertical sensitivities (column averaging kernels) for satellite observations of atmospheric methane in the SWIR and in the TIR. Adapted from Worden et al. (2015).

Atmos. Chem. Phys. Discuss., https://doi.org/10.5194/acp-2018-467
Manuscript under review for journal Atmos. Chem. Phys.
Discussion started: 29 May 2018

Atmospheric Chemistry and Physics Discussions

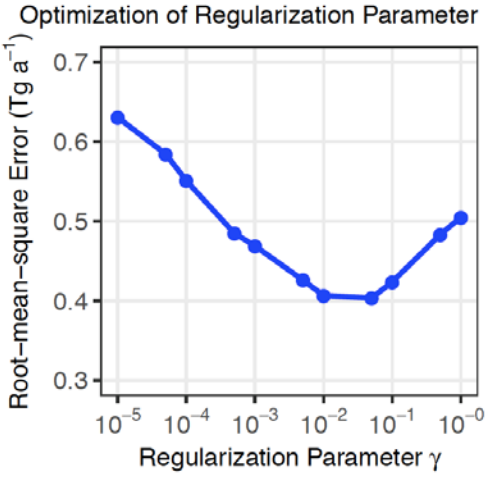

Figure 4 Ability of the inversion to match the "true" gridded methane emission field as a function of the regularization parameter γ in equation (4) for the SWIR+TIR satellite observing system. The ability is measured by the RMSE.

Atmos. Chem. Phys. Discuss., https://doi.org/10.5194/acp-2018-467
Manuscript under review for journal Atmos. Chem. Phys.
Discussion started: 29 May 2018

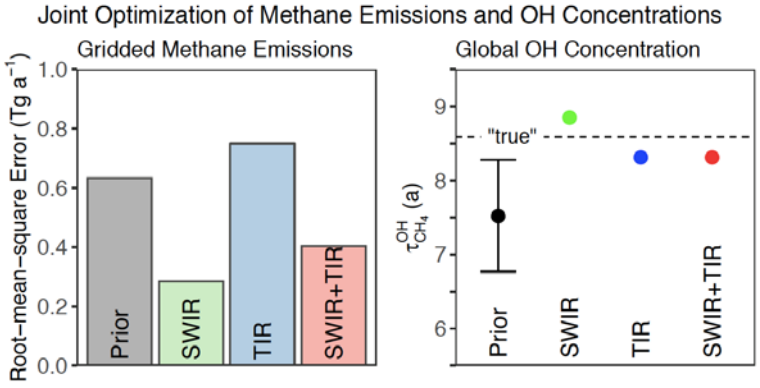

Figure 5 Ability of SWIR, TIR, and SWIR+TIR systems to jointly constrain gridded methane emissions and global OH concentrations (as measured by the methane lifetime $\tau^{OH}_{CH_4}$) in our base 1-year inversion. The left panel shows the RMSE in fitting the "true" 4°x5° gridded emission rates. The right panel compares the posterior estimates of $\tau^{OH}_{CH_4}$ to the prior estimate and to the "true" value. The prior error standard deviation is shown as a vertical bar. Posterior error bars are too small to be shown, although this reflects overoptimistic error characterization in the inversion (see text).

Atmos. Chem. Phys. Discuss., https://doi.org/10.5194/acp-2018-467
Manuscript under review for journal Atmos. Chem. Phys.
Discussion started: 29 May 2018

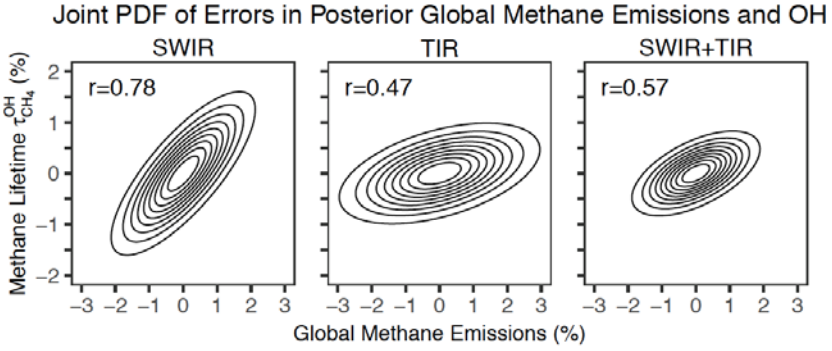

Figure 6 Joint distribution of relative uncertainties in $\tau_{CH_4}^{OH}$ and total methane emissions, summarized from posterior error covariance matrices, for different satellite observing systems. Contours represent confidence ellipses from probability 0.1 (innermost) to 0.9 (outermost) at an interval of 0.1. The correlation coefficients (*r*) between errors in $\tau_{CH_4}^{OH}$ and total methane emissions are inset.

Atmos. Chem. Phys. Discuss., https://doi.org/10.5194/acp-2018-467
Manuscript under review for journal Atmos. Chem. Phys.
Discussion started: 29 May 2018

Atmospheric Chemistry and Physics Discussions

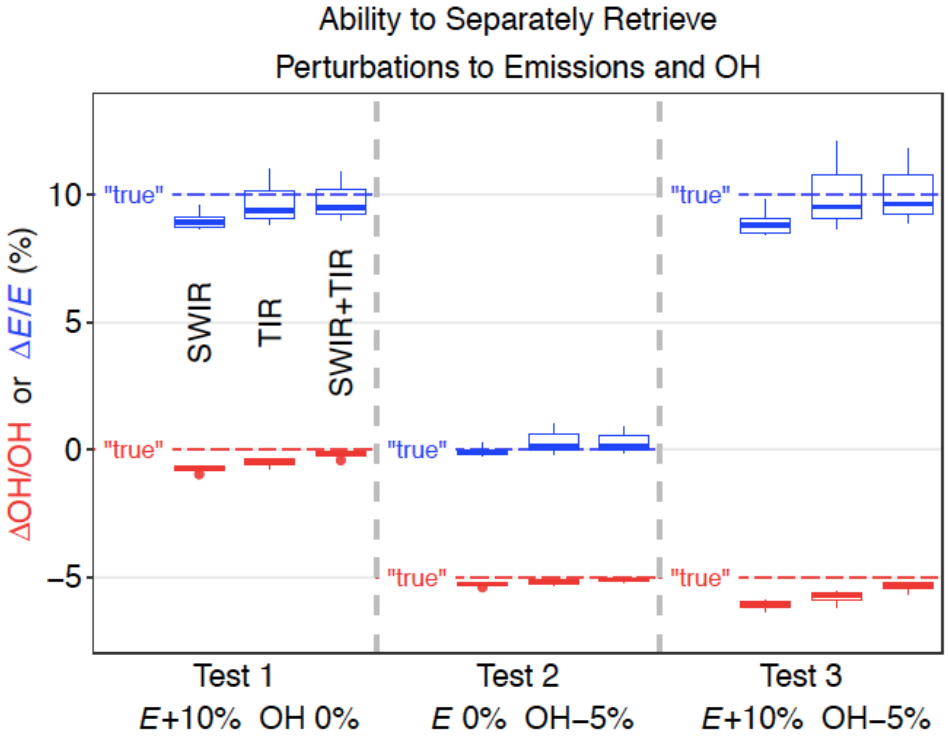

Figure 7 OSSE experiments perturbing global emissions (E+10%), OH (OH-5%), and both (E+10% OH-5%) to test whether the inversion can retrieve separately these perturbations. Results are shown for different satellite observing systems (SWIR, TIR, and SWIR+TIR). Blue symbols represent posterior estimation of changes in emissions and red symbols posterior estimation of change in global OH concentration. The boxes represent the 75th, 50th, and 25th percentiles and the whiskers represent the maximum and minimum of the results using 12 different OH distributions in "true" simulations. Dashed lines are "true" changes in global emissions (blue) and OH concentration (red).

Atmos. Chem. Phys. Discuss., https://doi.org/10.5194/acp-2018-467
Manuscript under review for journal Atmos. Chem. Phys.
Discussion started: 29 May 2018

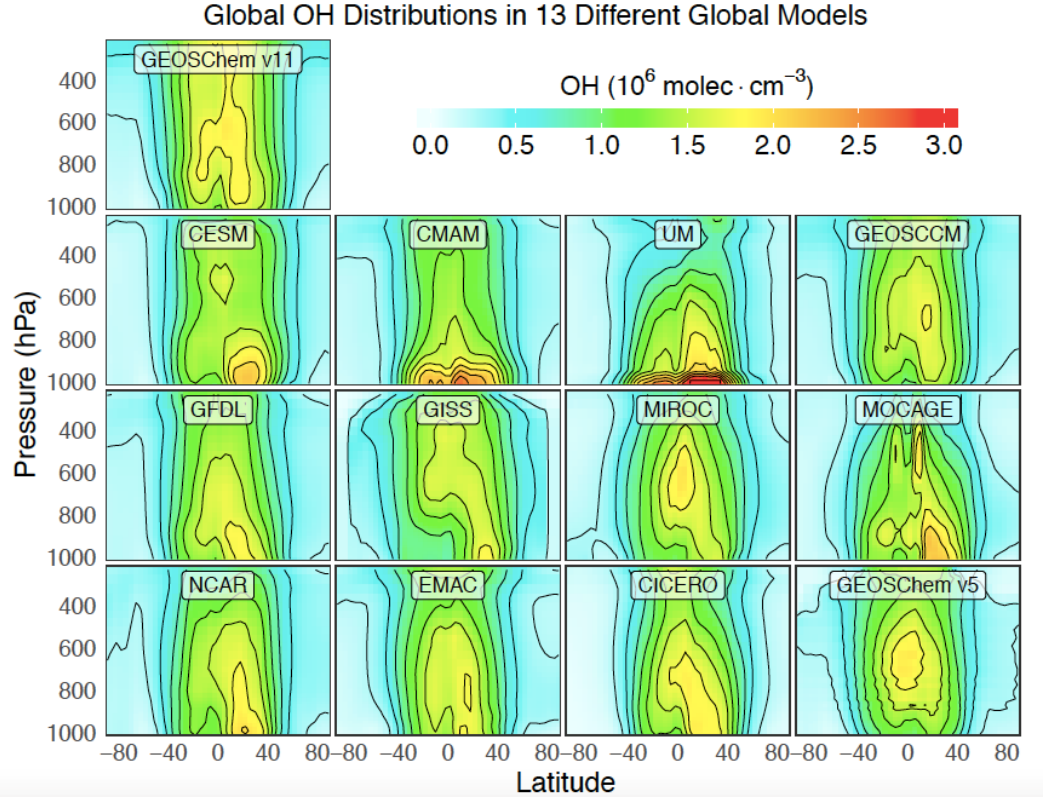

Figure 8 Variability of OH distributions across global models. The figure shows annual zonal mean OH concentrations for 13 different models used in the OSSE. GEOS-Chem v11 is used in the forward model for the inversion with $\tau_{CH_4}^{OH}$ = 7.5 years. GEOS-Chem v5 is used for the baseline "true" atmosphere with $\tau_{CH_4}^{OH}$ = 8.6 years. The other 11 distributions are from the ACCMIP model ensemble (Naik et al., 2013), with global scaling factors to impose $\tau_{CH_4}^{OH}$ = 8.6 years in all cases, and are used in alternative representations of the "true" atmosphere.

Atmos. Chem. Phys. Discuss., https://doi.org/10.5194/acp-2018-467
Manuscript under review for journal Atmos. Chem. Phys.
Discussion started: 29 May 2018

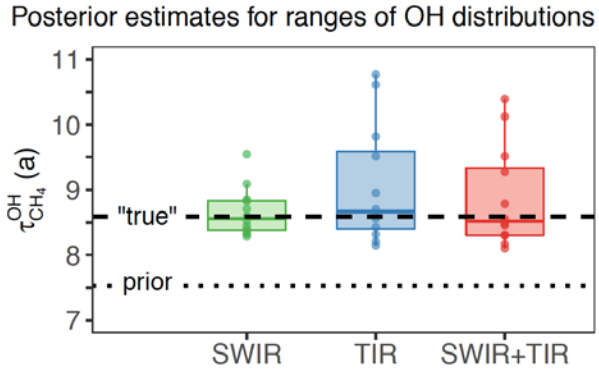

Figure 9 Effect of error in OH distribution on the optimization of the global OH concentration (methane lifetime $\tau^{OH}_{CH_4}$) from satellite observations. The Figure shows the posterior estimation of $\tau^{OH}_{CH_4}$ using 12 different OH distributions in simulations of the "true" atmosphere sampled by SWIR, TIR, and SWIR+TIR instruments, in comparison with "true" (dashed line) and prior (dotted line) $\tau^{OH}_{CH_4}$. The boxes represent the 75th, 50th, and 25th percentiles, the whiskers represent the maximum and minimum, and dots represent results for each OH distribution.

Atmos. Chem. Phys. Discuss., https://doi.org/10.5194/acp-2018-467
Manuscript under review for journal Atmos. Chem. Phys.
Discussion started: 29 May 2018

Atmospheric Chemistry and Physics Discussions

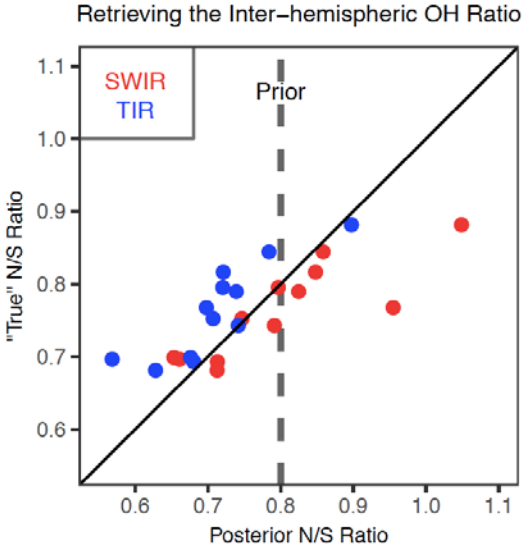

Figure 10 Ability of the inversion of satellite methane observations to retrieve the interhemispheric OH ratio defined by $\tau_{CH_4}^{OH,NH}/\tau_{CH_4}^{OH,SH}$. Posterior inversion results using either SWIR or TIR observations are compared to the "true" ratio from 12 different model OH distributions (Figure 8). The dashed vertical line represents the prior $\tau_{CH_4}^{OH,NH}/\tau_{CH_4}^{OH,SH}$ common to all inversions.